SIAM J. SCI. COMPUT.
Vol. 42, No. 4, pp. A2014–A2036

NUMERICAL UPSCALING OF PERTURBED DIFFUSION PROBLEMS*

FREDRIK HELLMAN†, TIM KEIL‡, AND AXEL MÅLQVIST†

Abstract. In this paper we study elliptic partial differential equations with rapidly varying diffusion coefficient that can be represented as a perturbation of a reference coefficient. We develop a numerical method for efficiently solving multiple perturbed problems by reusing local computations performed with the reference coefficient. The proposed method is based on the Petrov–Galerkin localized orthogonal decomposition (PG-LOD), which allows for straightforward parallelization with low communication overhead and memory consumption. We focus on two types of perturbations: local defects, which we treat by recomputation of multiscale shape functions, and global mappings of a reference coefficient for which we apply the domain mapping method. We analyze the proposed method for these problem classes and present several numerical examples.

Key words. finite element method, multiscale method, LOD, Petrov–Galerkin, composite material, random perturbations

AMS subject classifications. 35J15, 65N12, 65N30

DOI. 10.1137/19M1278211

1. Introduction.

Manufactured heterogeneous materials, such as composites with tailored properties, are crucial tools in engineering. The challenge of performing accurate computer simulations involving such materials have driven the development of multiscale methods over decades [7, 18, 19, 23, 25]. Multiscale methods have turned out to be successful in computing coarse-scale representations of the solutions to such problems. However, when the heterogeneous data is perturbed it is not obvious how multiscale methods can be adapted. Understanding the effect of perturbations is important since manufactured materials, in general, will not be perfect. Manufacturing tolerances and defects lead to perturbations in the material distribution. There are also other problems, such as time stepping with time dependent diffusion coefficient, optimization of material distribution, and nonlinear diffusion problems, which call for iterative procedures where the data in the current iteration can be seen as a perturbation of the data in the previous iteration.

In this paper, we study elliptic problems with diffusion coefficients that are perturbations of a single reference diffusion coefficient. We consider the following Dirichlet type problem, which we will refer to as the strong form of the (inhomogeneous) *perturbed problem*: find $\bar{u}$ such that

$$\begin{aligned} -\nabla \cdot A\nabla \bar{u} &= f \qquad \text{in } \Omega, \\ \bar{u} &= g \qquad \text{on } \Gamma \end{aligned} \tag{1.1}$$

*Submitted to the journal's Methods and Algorithms for Scientific Computing section August 1, 2019; accepted for publication (in revised form) April 15, 2020; published electronically July 6, 2020.
https://doi.org/10.1137/19M1278211

Funding: The work of the first and third authors was supported by the Swedish Research Council through grant 2015-04964 and by the Goran Gustafsson Foundation. The second authors work was funded by Deutsche Forschungsgemeinschaft (DFG, German Research Foundation) under Germany's Excellence Strategy – EXC 2044 – 390685587, Mathematics Münster and by the DFG under contract OH 98/11-1.

†Department of Mathematical Sciences, Chalmers University of Technology and University of Gothenburg SE-421 96 Göteborg, Sweden (fredrik.hellman@gmail.com, axel@chalmers.se).

‡Institute for Computational and Applied Mathematics, Westfälische Wilhelms-Universität Münster, Einsteinstraße 62, D-48149 Münster, Germany (tim.keil@uni-muenster.de).

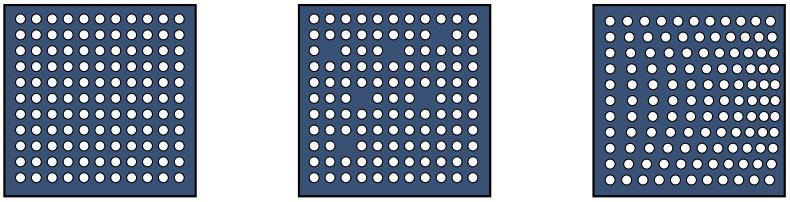

FIG. 1. *The pictures illustrate $A_{ref}(x)$ (left) taking two values in the computational domain, random defects (center), and domain mapping of the reference (right).*

on a bounded polygonal/polyhedral domain $\Omega \subset \mathbb{R}^d$, $d = 2, 3$, with boundary Γ. We assume the right-hand side $f \in L^2(\Omega)$, diffusion coefficient $A \in L^\infty(\Omega, \mathbb{R}^{d\times d})$ is symmetric positive definite and rapidly varying, and the trace of the function $g \in H^1(\Omega)$ defines the Dirichlet boundary conditions. We further consider A and f to be a perturbations of a reference diffusion coefficient and a reference right-hand side, respectively,

$$A(x) \approx A_{\text{ref}}(x), \qquad f(x) \approx f_{\text{ref}}(x). \tag{1.2}$$

The aim of the paper is to reuse computations made with the reference quantities A_{ref} and f_{ref} in a reliable way when solving a set of perturbed problems. The perturbations we study are local defects and domain mappings. Figure 1 illustrates the reference coefficient (left), random defects (center), and domain mapping to the physical diffusion coefficient (right).

Perturbations of the diffusion coefficient in elliptic problems have been studied extensively. This work was inspired by a series of papers by Le Bris and coworkers on weakly random homogenization [2, 3, 21, 22], where they consider problems with randomly perturbed periodic coefficients, similar to the ones illustrated in Figure 1, i.e., with local defects and deformations of the periodic structure. This allows the authors to consider both rapidly varying and perturbed diffusion coefficients. There are several works on partial differential equations posed on random domains using domain mapping including [5, 12, 29].

While this paper shares some aspects of the problem settings (such as considering defects and deformed domains) with the previously mentioned works, it deviates from the themes of randomness and analytic homogenization by considering deterministic numerical homogenization of elliptic problems. The main difference in terms of problem setting from the preceding work [16] is that the paper at hand considers a single reference coefficient (as opposed to a reference coefficient evolving in time) and, perhaps more importantly, that it introduces a way to handle deformed coefficients by means of domain mappings. This gives a method that can be used to reduce the computational work when many problems with similar coefficients are generated, for example, in Monte Carlo sampling. Examples of elliptic problems with deformed multiscale coefficients appear in simulation of so called meta-materials. They are manufactured materials with tailored macroscopic material properties. See [30] for a recent review over that field and [10, 28] for two examples of meta-material studies. The proposed method handles both deformed coefficients and defects in a unified manner.

Multiscale methods have been a vibrant area of research for decades [1, 7, 18, 25]. The main idea is to solve local fine scale problems to compute an improved basis which is used to solve a global coarse-scale problem. These techniques are often

parallel by construction. One method that has proven to give accurate results also for nonperiodic diffusion coefficient is the localized orthogonal decomposition (LOD) method [23]. LOD is based on an orthogonal split of the solution space, using the scalar product induced by the weak form of the problem (1.1). In recent years it has been improved and reformulated. In [8] a Petrov–Galerkin version of the method was presented and analyzed. PG-LOD has the advantage that the assembly of the modified stiffness matrix is much faster than for the symmetric Galerkin method. Concerning the implementation of the LOD, a detailed algebraic overview has been given in [9]. In the recent work [16] a sequence of problems with similar coefficients are considered, with applications in time dependent diffusion problems. This approach is also useful for studying perturbations of the type presented in Figure 1 (see [20]).

In this paper we apply the PG-LOD methodology introduced in [16] to solve elliptic problems with perturbed diffusion coefficient. The PG-LOD method allows for local recomputation of basis functions to handle perturbations in the data from defects and domain mappings. We derive error indicators to decide where recomputations are necessary. In this way we can efficiently simulate a vast number of perturbations by mainly solving upscaled coarse-scale problems.

The paper is organized as follows. In section 2 we formulate the problem and the types of perturbations that are considered in this paper. In section 3 we present the proposed numerical method based on PG-LOD. In section 4 we derive error bounds, and in section 5 we discuss implementation, memory consumption, and parallelization. Finally, in section 6 we present numerical examples.

2. Problem formulation. We assume that the matrix $A \in L^\infty(\Omega, \mathbb{R}^{d\times d})$ is symmetric and uniformly elliptic such that

$$0 < \alpha := \operatorname{ess\,inf}_{x\in\Omega} \inf_{v\in\mathbb{R}^d\setminus\{0\}} \frac{(A(x)v)\cdot v}{v\cdot v}, \tag{2.1}$$

$$\infty > \beta := \operatorname{ess\,sup}_{x\in\Omega} \sup_{v\in\mathbb{R}^d\setminus\{0\}} \frac{(A(x)v)\cdot v}{v\cdot v}. \tag{2.2}$$

We further let $f \in L^2(\Omega)$ and $g \in H^1(\Omega)$ with a trace on Γ which defines the Dirichlet boundary values. We introduce a function space V where we seek a solution of (1.1) posed on variational form. In this paper we consider a conforming finite element space

$$V := V_h \subset H_0^1(\Omega) = \{v \in H^1(\Omega) \mid \operatorname{tr}(v) = 0\},$$

defined on a computational mesh $\mathcal{T}_h$ that is assumed to be fine enough to resolve the variations in the diffusion coefficients well. However, we may as well choose $V = H_0^1(\Omega)$ and the analysis presented in the paper will still go through. To simplify the notation we stick to the notation $u \in V = V_h$. On weak form we get the following: find $u \in V$ such that

$$a(u, v) = F(v) - a(g, v) \tag{2.3}$$

for all $v \in V$, where

$$a(u, v) := \int_\Omega (A\nabla u)\cdot\nabla v, \qquad F(v) := \int_\Omega fv. \tag{2.4}$$

The Lax–Milgram lemma guarantees the existence and uniqueness of a solution $u \in V$. The full solution including the boundary data is given by $u + g$. As mentioned above, (2.3) will be referred to as the *perturbed problem*.

To motivate why we cannot simply replace the perturbed coefficient with the reference coefficient, we formulate an artificial problem based on the reference coefficient and right-hand side: find $u_{\text{ref}} \in V$, such that for all $v \in V$,

$$\int_\Omega A_{\text{ref}} \nabla(u_{\text{ref}} + g) \cdot \nabla v \, dx = \int_\Omega f_{\text{ref}} \, v. \tag{2.5}$$

The error between u_{ref} and u can be bounded in the energy norm $|||\cdot||| := a(\cdot,\cdot)^{1/2} = \|A^{1/2}\nabla\cdot\|_{L^2(\Omega)}$ in the following way:

$$\begin{aligned} |||u - u_{\text{ref}}|||^2 &\leq (A\nabla u - A_{\text{ref}}\nabla u_{\text{ref}}, \nabla(u - u_{\text{ref}})) + (A_{\text{ref}}\nabla u_{\text{ref}} - A\nabla u_{\text{ref}}, \nabla(u - u_{\text{ref}})) \\ &= (f - f_{\text{ref}}, u - u_{\text{ref}}) + ((A_{\text{ref}} - A)\nabla(u_{\text{ref}} + g), \nabla(u - u_{\text{ref}})) \\ &\leq \left(\frac{C_{\text{P}}}{\alpha^{1/2}} \|f - f_{\text{ref}}\|_{L^2(\Omega)} + \frac{C_{\text{P}}}{\alpha^{3/2}} \|A_{\text{ref}} - A\|_{L^\infty(\Omega)} \|f_{\text{ref}}\|_{L^2(\Omega)} \right) |||u - u_{\text{ref}}|||, \end{aligned} \tag{2.6}$$

where C_{P} is the Poincaré constant for Ω. This error bound suggests that even local perturbations in the structure of the coefficient or the right-hand side, e.g., by a defect or shift, may lead to very poor accuracy. This occurs, for example, if we consider a problem with a highly conductive thin channel in the diffusion coefficient and a right-hand side f which has support inside the channel. If the channel is moved slightly so that the support of the right-hand side is now outside the channel, the solution will behave very differently. The error with respect to perturbations in f is less severe since it is measured in the L^2-norm.

For this reason it is not clear how to reuse computations for the standard finite element method in a reliable way. In this paper we will treat this difficulty using a multiscale approach where solutions to localized subproblems, based on the reference coefficient, can be reused when solving for the perturbed problem.

2.1. Perturbations. To simplify the presentation we consider perturbations of coefficients that only take the two values 1 and $0 < \alpha < 1$. We emphasize that this is not necessary for the proposed method to work or for theory to hold and we do consider diffusion coefficients that vary continuously in two of the numerical examples. However, it highlights the application to composite materials which has inspired this work. Let $\Omega_1, \Omega_\alpha \subseteq \Omega$ be two disjoint subdomains of Ω with $\Omega_1 \cup \Omega_\alpha = \Omega$. Let A_{ref} be defined by

$$A_{\text{ref}} = \chi_{\Omega_1} + \alpha\chi_{\Omega_\alpha}, \tag{2.7}$$

where χ is an indicator function.

We formalize the two types of perturbations that we consider (see Figure 1) by introducing a defect perturbation D and a domain mapping ψ. A perturbation from a defect can be expressed by $D = (1 - \alpha)\chi_\omega$, where $\omega \subseteq \Omega_1$ and $A_{\text{ref}} - D$ can be considered as the perturbed coefficient. For shift perturbations, we assume that the domain mapping perturbation can be described as a variable transformation with a perturbation function $\psi : \Omega \to \Omega$ which maps the reference coefficient (expressed in x-coordinates) to a mapped coefficient (expressed in y-coordinates). We assume that ψ maps the boundary to itself (i.e., $\Gamma = \{\psi(x) : x \in \Gamma\}$) and that it is a one-to-one mapping in Ω. Figure 2 provides an example of a variable transformation. We denote the corresponding Jacobi matrix

$$\mathcal{J}_{ij}(x) = \left[\frac{\partial \psi_i}{\partial x_j} \right]$$

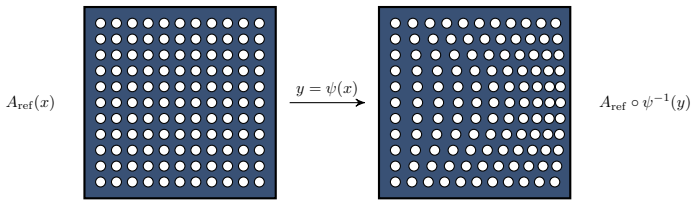

FIG. 2. *Illustration of a domain mapping ψ with $D \equiv 0$.*

for $1 \leq i, j \leq d$, and assume it to be bounded with bounded inverse for a.e. $x \in \Omega$. The two perturbation types can either be combined or be considered individually by letting $D \equiv 0$ or $\psi = \mathrm{Id}$.

Using A_{ref}, D, and ψ, we formulate the *mapped problem* in the y-variable with $y = \psi(x)$ by

$$\begin{aligned} -\nabla_y \cdot A_y \nabla_y u_y &= f_y \qquad \text{in } \Omega, \\ u_y &= g_y \qquad \text{on } \Gamma, \end{aligned} \tag{2.8}$$

where the coefficient is defined by $A_y = (A_{\text{ref}} - D) \circ \psi^{-1}$, and the derivatives have been distorted accordingly. The y-variable corresponds to the physical spatial variable in a typical situation. Depending on the physics being modeled, either the mapped right-hand side $f_y \in L^2(\Omega)$ or the perturbed f (below) can be considered given. It makes no difference for the development of the numerical method but may affect the choice of f_{ref}. The Dirichlet boundary value $g_y \in H^{1/2}(\Gamma)$ is defined only on the boundary Γ, which is mapped to itself. The solution in the perturbed domain is denoted $u_y(y)$.

Next, we use the mapped problem to define the perturbed problem in (2.3). The gradient operator ∇_y in the mapped domain can be expressed in $\nabla_x = \nabla$ by

$$\nabla_y v(x) := \left[\frac{\partial v}{\partial y_i}(x) \right]_i = \left[\sum_j \frac{\partial v}{\partial x_j}(x) \frac{\partial x_j}{\partial y_i}(x) \right]_i = \mathcal{J}^{-T}(x) \nabla_x v(x). \tag{2.9}$$

Based on the elliptic operator in (2.8) we define the perturbed bilinear form for the mapped problem as

$$\begin{aligned} a(v, w) &= \int_\Omega \left((A_{\text{ref}} - D) \circ \psi^{-1} \right) \nabla_y \left(v \circ \psi^{-1} \right) \cdot \nabla_y \left(w \circ \psi^{-1} \right) \, \mathrm{d}y \\ &= \int_\Omega \det(\mathcal{J}) \mathcal{J}^{-1} (A_{\text{ref}} - D) \mathcal{J}^{-T} \nabla_x v \cdot \nabla_x w \, \mathrm{d}x \end{aligned}$$

and the corresponding linear functional

$$F(w) = \int_\Omega f_y \left(w \circ \psi^{-1} \right) \, \mathrm{d}y = \int_\Omega \det(\mathcal{J}) \left(f_y \circ \psi \right) w \, \mathrm{d}x.$$

We see that this now fits the formulation of the perturbed problem (2.3) with

$$A = \det(\mathcal{J}) \mathcal{J}^{-1} (A_{\text{ref}} - D) \mathcal{J}^{-T}, \qquad f = \det(\mathcal{J}) \left(f_y \circ \psi \right), \qquad g|_\Gamma = g_y \circ \psi,$$

and mapped solution $u_y = (u + g) \circ \psi^{-1}$. For the problem to be well posed we assume $\mathcal{J}$ and $\mathcal{J}^{-1}$ to be bounded almost everywhere and A to be symmetric positive

definite. We note that the perturbed coefficient A can be computed from the reference coefficient by means of the Jacobian matrix and that the Dirichlet boundary value function $g \in H^1(\Omega)$ can be chosen arbitrarily in the interior of Ω. We emphasize that the domain mapping transforms a shift defect to a change-in-value perturbation. For many coefficients this is advantageous as seen in (2.6), where now the L^∞-norm can be expressed entirely in terms of how much $\mathcal{J}$ differs from identity. The domain mapping covers continuous (possibly global) perturbations while defects cover discontinuous (often local) perturbations. With respect to Figure 1 we see that the middle picture corresponds to $\psi = \mathrm{Id}$ and the right picture to $D \equiv 0$.

Remark 2.1 (discretization of ψ). In the numerical examples in section 6 we let $V = V_h$ be the space of quadrilateral finite elements and ψ to be a linear combination of the corresponding bilinear shape functions. This leads to an isoparametric finite element formulation. Isoparametric finite elements are, for instance, used to guarantee accuracy when solving problems on curved domains. Here the aim is instead to map the perturbed diffusion coefficient to a reference. The theoretical justification for using bilinear domain mappings ψ follows directly from the theory of isoparametric finite elements (see [4, 6]).

3. Adaptive PG-LOD method. In this section, we develop the proposed method that reuses reference computations peformed using the reference coefficient A_{ref} and right-hand side f_{ref} in an adaptive manner to solve the perturbed problem (2.3) expressed in A, u, f, and g. The perturbed data can stem from a domain mapping, defects, or both. We consider the Petrov–Galerkin version of the LOD method as presented in [8] and briefly derive it in sections 3.1–3.3. Section 3.4 defines the computable error indicators, and section 3.5 presents the method that reuses reference computations while balancing the error.

3.1. Preliminaries. Let $\mathcal{T}_H$ be a coarse, shape regular, conforming mesh family of the domain Ω. We denote the maximum diameter of an element in $\mathcal{T}_H$ with H and $\mathcal{N}$ the set of all corresponding interior nodes of the mesh $\mathcal{T}_H$. We let

$$V_H := V \cap \mathcal{P}_1(\mathcal{T}_H),$$

where $\mathcal{P}_1(\mathcal{T}_H)$ denotes the space of $\mathcal{T}_H$-piecewise affine functions that are continuous on the domain Ω. Since our full space V is a conforming finite element space we assume that the meshes and spaces are nested $V_H \subset V$. However, it is possible, with a minor modification of the proposed method, to violate this condition and still get convergence (see [24]).

We introduce the concept of element patches as they will be used in the definition of the interpolation and for the localization of the PG-LOD method. For arbitrary $\omega \subseteq \Omega$ and $0 \leq k \in \mathbb{N}$, we define coarse grid patches $U_k(\omega) \subset \Omega$ by

$$\begin{aligned} U_0(\omega) &= \omega, \\ U_{k+1}(\omega) &= \bigcup \Big\{ T \in \mathcal{T}_H \,\Big|\, \overline{U_k(\omega)} \cap \overline{T} \neq 0 \Big\}. \end{aligned}$$

If $\omega = \{x\}$, for a node $x \in \mathcal{N}$, we call $U_k(x)$ a k-layer nodal patch. For $\omega = T$, where $T \in \mathcal{T}_H$, we call $U_k(T)$ a k-layer element patch (see Figure 3).

3.2. Multiscale decomposition. Fine scale features that occur in the solutions are not captured in the space V_H. We characterize the fine scale parts of V as the kernel of an linear surjective (quasi-)interpolation operator $\mathcal{I}_H : V \to V_H$ that maps

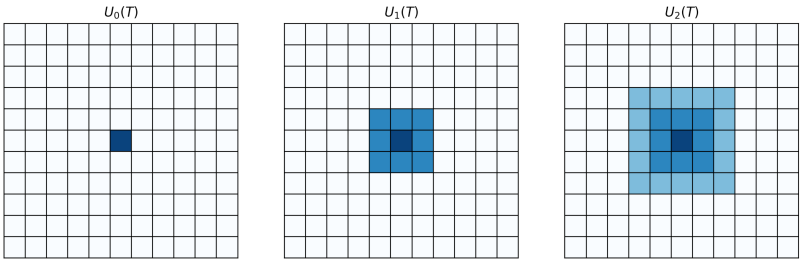

FIG. 3. *Patches for a coarse mesh element $T \in \mathcal{T}_H$.*

a function $v \in V$ to a function $v_H \in V_H$ in the coarse FE space. Let $\mathcal{T}_x = \{T \in \mathcal{T}_H : x \in \overline{T}\}$ be the set of elements neighboring x. We let the interpolation operator $\mathcal{I}_H : V \to V_H$ be an L^2-projection to the broken finite element space in composition with averaging in the nodes. In other words,

$$\mathcal{I}_H v := \sum_{x \in \mathcal{N}} \zeta_x \lambda_x,$$

where coefficients ζ_x are determined as follows. Let the operator P_T be the element L^2-projection $P_T v \in V_H\big|_T$ such that

$$\int_T (P_T v) w_H = \int_T v w_H$$

for all $w_H \in V_H\big|_T$, and then

$$\zeta_x = \operatorname{card}(\mathcal{T}_x)^{-1} \sum_{T' \in \mathcal{T}_x} (P_{T'} v)(x).$$

This interpolation operator is linear and continuous and its restriction to V_H is an isomorphism. Furthermore it fulfills the stability result

$$H_T^{-1} \|v - \mathcal{I}_H v\|_{L^2(T)} + \|\nabla \mathcal{I}_H v\|_{L^2(T)} \leq C_{\mathcal{I}_H} \|\nabla v\|_{L^2(U_1(T))} \tag{3.1}$$

for every $v \in V$ and $T \in \mathcal{T}_H$, with a generic constant $C_{\mathcal{I}_H} > 0$ (see [26]). We refer to [15, 27] for other possible choices of interpolation operators.

We let the kernel of $\mathcal{I}_H$,

$$V^{\mathrm{f}} = \ker(\mathcal{I}_H) = \{v \in V \,|\, \mathcal{I}_H(v) = 0\},$$

define the fine scales of the space V. Since $\mathcal{I}_H$ is a projection, this allows for the split $V = V_H \oplus V^{\mathrm{f}}$. We define a correction operator $\mathcal{Q}v \in V^{\mathrm{f}}$, for a given $v \in V$, to be the solution of

$$a(\mathcal{Q}v, v^{\mathrm{f}}) = a(v, v^{\mathrm{f}})$$

for all $v^{\mathrm{f}} \in V^{\mathrm{f}}$, and define the multiscale space $V^{\mathrm{ms}} := V_H - \mathcal{Q}V_H$.

For any $v^{\mathrm{f}} \in V^{\mathrm{f}}$ and $v^{\mathrm{ms}} \in V^{\mathrm{ms}}$, we observe $a(v^{\mathrm{ms}}, v^{\mathrm{f}}) = 0$. This leads to the orthogonal decomposition with respect to the a-scalar product, $V = V^{\mathrm{ms}} \oplus_a V^{\mathrm{f}}$. Right-hand correction can be used to improve accuracy in LOD based methods (see, e.g., [16, 17]). We define this correction by $\mathcal{R}f \in V^{\mathrm{f}}$ such that, for all $v^{\mathrm{f}} \in V^{\mathrm{f}}$,

$$a(\mathcal{R}f, v^{\mathrm{f}}) = \int_\Omega f v^{\mathrm{f}}.$$

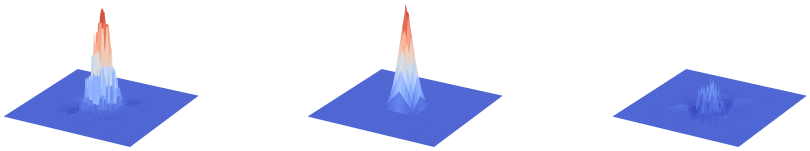

(a) $\lambda_x - \mathcal{Q}\lambda_x$. (b) λ_x. (c) $\mathcal{Q}\lambda_x$.

FIG. 4. *Basis function of V_H^{ms} and its decomposition for $x \in \mathcal{N}$.*

We now derive the Petrov–Galerkin LOD method for the perturbed problem (see also [8, 11]). We use $V = V_H \oplus V^{\mathrm{f}}$ to decompose (2.3) into two equations:

$$a(u_H + u^{\mathrm{f}}, v_H) = F(v_H) - a(g, v_H), \tag{3.2}$$

$$a(u^{\mathrm{f}}, v^{\mathrm{f}}) = F(v^{\mathrm{f}}) - a(g, v^{\mathrm{f}}) - a(u_H, v^{\mathrm{f}}) \tag{3.3}$$

for all $v_H \in V_H$ and $v^{\mathrm{f}} \in V^{\mathrm{f}}$.

With the definitions of $\mathcal{Q}$ and $\mathcal{R}$ we obtain from (3.3) that $u^{\mathrm{f}} = -\mathcal{Q}u_H + \mathcal{R}f - \mathcal{Q}g$. Plugging this into (3.2) gives

$$a(u^{\mathrm{ms}}, v_H) = F(v_H) - a(\mathcal{R}f, v_H) - a(g - \mathcal{Q}g, v_H) \tag{3.4}$$

for all $v_H \in V_H$. Hence, solving (3.4) gives the exact solution $u = u^{\mathrm{ms}} + \mathcal{R}f - \mathcal{Q}g$.

In order to use the multiscale space in a practical implementation, we need a computable basis. Since V^{ms} and V_H have equal dimensions, it suffices to apply the fine scale corrector $\mathcal{Q}$ on every single basis function λ_x of V_H to obtain a corrected basis, i.e.,

$$\{\lambda_x - \mathcal{Q}\lambda_x \,|\, x \in \mathcal{N}\}.$$

We note that a global fine scale computation for each node is necessary to compute all $\mathcal{Q}\lambda_x$, which is computationally expensive. However, Figure 4 suggests that the computation can be localized to a small area around the support of the original basis function. It was shown in [23] that the corrected basis functions decay exponentially and that localized computations are possible.

Remark 3.1 (mixed boundary conditions). It is also possible to have mixed Neumann and Dirichlet boundary conditions in the PG-LOD method (see [17]). With mixed boundary conditions we also need to compute fine scale corrections for the inhomogeneous Neumann boundary data (as we do for the Dirichlet data) to get optimal convergence rate.

3.3. Localized multiscale method. The fine scale space V^{f} can be restricted to patches $U_k(\omega)$ with the intuitive definition, for $\omega \subseteq \Omega$ and $k \in \mathbb{N}$,

$$V^{\mathrm{f}}(U_k(\omega)) := \left\{ v \in V^{\mathrm{f}} \,\middle|\, v|_{\Omega \setminus U_k(\omega)} = 0 \right\}.$$

These local fine scale patches enable the truncation of the corrector. We define localized element correction operators $\mathcal{Q}_k$ and $\mathcal{R}_k$ by

$$\mathcal{Q}_k v := \sum_{T \in \mathcal{T}_H} \mathcal{Q}_{k,T} v, \qquad \text{and} \qquad \mathcal{R}_k f := \sum_{T \in \mathcal{T}_H} \mathcal{R}_{k,T} f,$$

where $\mathcal{R}_{k,T}, \mathcal{Q}_{k,T} : V \to V^{\mathrm{f}}(U_k(T))$ solves

$$a(\mathcal{Q}_{k,T}v, v^{\mathrm{f}}) = \int_T A\nabla v \cdot \nabla v^{\mathrm{f}},$$
$$a(\mathcal{R}_{k,T}f, v^{\mathrm{f}}) = \int_T f\, v^{\mathrm{f}}$$

for all $v^{\mathrm{f}} \in V^{\mathrm{f}}(U_k(T))$. We construct a localized multiscale space V_k^{ms} using V_H and the local correctors

$$V_k^{\mathrm{ms}} := V_H - \mathcal{Q}_k V_H.$$

This space is spanned by $\{\lambda_x - \mathcal{Q}_k\lambda_x\}_{x\in\mathcal{N}}$.

We formulate the localized version of the PG-LOD in (3.4): find $u_k^{\mathrm{ms}} \in V_k^{\mathrm{ms}}$ such that for all $v \in V_H$,

$$a(u_k^{\mathrm{ms}}, v) = F(v) - a(\mathcal{R}_k f, v) - a(g - \mathcal{Q}_k g, v), \tag{3.5}$$

where the full approximation of u is

$$u_k = u_k^{\mathrm{ms}} + \mathcal{R}_k f - \mathcal{Q}_k g = u_k^H - \mathcal{Q}_k u_k^H + \mathcal{R}_k f - \mathcal{Q}_k g. \tag{3.6}$$

The main reason for using a Petrov–Galerkin formulation is that it avoids the expensive computation of products between corrected basis functions without losing convergence order [8].

The exponential decay of the correctors yield the following error bounds (see [23]) of the localized correctors in terms of $k \in \mathbb{N}$:

$$|||(\mathcal{Q} - \mathcal{Q}_k)v||| \lesssim k^{d/2}\theta^k |||v||| \qquad \text{and} \qquad |||(\mathcal{R} - \mathcal{R}_k)f||| \lesssim k^{d/2}\theta^k \|f\|_{L^2(\Omega)}, \tag{3.7}$$

where $0 < \theta < 1$ is independent of H, k, but generally depends, e.g., on the contrast of the coefficient and the choice of interpolation operator. See [15, 16, 23] for more details on θ. Moreover, the notation $a \lesssim b$ means $a \le Cb$ with a constant C, independent of H, k and later in the manuscript also TOL and τ (to be defined below). The well-posedness of (3.5) was studied previously in [8, 16] and appears to be conditioned on sufficiently large k in general. (This condition will be revisited in the proof of Theorem 4.1). Furthermore, from [16, section 4.2] we obtain an error bound for $u - u_k$, which reads

$$|||u - u_k||| \lesssim |||(\mathcal{Q} - \mathcal{Q}_k)(\mathcal{I}_H u + g)||| + |||(\mathcal{R} - \mathcal{R}_k)f||| \lesssim k^{d/2}\,\theta^k \left(\|f\|_{L^2(\Omega)} + |||g|||\right). \tag{3.8}$$

3.4. Error indicators. Since the aim of this paper is to reuse local corrector computations performed with the reference coefficients A_{ref} and f_{ref}, we need a notation for a modified $\mathcal{Q}_{k,T}$ and $\mathcal{R}_{k,T}$, computed using A_{ref} instead of A and f_{ref} instead of f. We let $\mathcal{Q}_{k,T}^{\mathrm{ref}} : V \to V^{\mathrm{f}}(U_k(T))$ and $\mathcal{R}_{k,T}^{\mathrm{ref}} : L^2(\Omega) \to V^{\mathrm{f}}(U_k(T))$ be the solutions to

$$(A_{\mathrm{ref}}\nabla\mathcal{Q}_{k,T}^{\mathrm{ref}}v, \nabla v^{\mathrm{f}}) = \int_T A_{\mathrm{ref}}\nabla v \cdot \nabla v^{\mathrm{f}},$$
$$(A_{\mathrm{ref}}\nabla\mathcal{R}_{k,T}^{\mathrm{ref}}f_{\mathrm{ref}}, \nabla v^{\mathrm{f}}) = \int_T f_{\mathrm{ref}} v^{\mathrm{f}}$$

for all $v^{\mathrm{f}} \in V^{\mathrm{f}}(U_k(T))$. In order to decide for which $T \in \mathcal{T}_H$ we need to recompute the correctors ($\mathcal{Q}_{k,T}$ and $\mathcal{R}_{k,T}$) and for which we can still use the reference correctors

($\mathcal{Q}^{\mathrm{ref}}_{k,T}$ and $\mathcal{R}^{\mathrm{ref}}_{k,T}$) we need computable error indicators. For the indicators to be useful and efficient they have to be computable and independent of $\mathcal{Q}_{k,T}$ and $\mathcal{R}_{k,T}$.

For every $T \in \mathcal{T}_H$ we define error indicators only depending on the reference corrector and coefficients A and A_{ref}. The definition of the error indicators is motivated by Lemma 4.2 and by Theorem 4.1 in section 4 below.

DEFINITION 3.2 (error indicators). *For each $T \in \mathcal{T}_H$, we define*

(3.9)

$$E^2_{\mathcal{Q}V_H,T} := \|A_{\mathrm{ref}}A^{-1}\|_{L^\infty(T)} \cdot \sum_{\substack{T'\in\mathcal{T}_H \\ T'\cap U_k(T)\neq 0}} \|\delta\|^2_{L^\infty(T')} \max_{w|_T,\, w\in V_H} \frac{\|A^{1/2}_{\mathrm{ref}}(\chi_T\nabla w - \nabla\mathcal{Q}^{\mathrm{ref}}_{k,T}w)\|^2_{L^2(T')}}{\|A^{1/2}_{\mathrm{ref}}\nabla w\|^2_{L^2(T)}},$$

$$E^2_{f,T} := \|A^{-1}\|_{L^\infty(U(T))} \sup_{v\in V} \frac{\|(\mathrm{Id}-\mathcal{I}_H)v\|^2_{L^2(T)}}{\|\nabla v\|^2_{L^2(U(T))}} \|f - f_{\mathrm{ref}}\|^2_{L^2(T)},$$

$$E^2_{\mathcal{R}f,T} := \|A_{\mathrm{ref}}A^{-1}\|_{L^\infty(T)} \sum_{\substack{T'\in\mathcal{T}_H \\ T'\cap U_k(T)\neq 0}} \|\delta\|^2_{L^\infty(T')} \|A^{1/2}_{\mathrm{ref}}\nabla\mathcal{R}^{\mathrm{ref}}_{k,T}f_{\mathrm{ref}}\|^2_{L^2(T')},$$

$$E^2_{\mathcal{Q}g,T} := \|A_{\mathrm{ref}}A^{-1}\|_{L^\infty(T)} \sum_{\substack{T'\in\mathcal{T}_H \\ T'\cap U_k(T)\neq 0}} \|\delta\|^2_{L^\infty(T')} \|A^{1/2}_{\mathrm{ref}}(\chi_T\nabla g - \nabla\mathcal{Q}^{\mathrm{ref}}_{k,T}g)\|^2_{L^2(T')},$$

where χ_T denotes the indicator function for an element $T \in \mathcal{T}_H$ and

$$\delta = A^{-1/2}(A - A_{\mathrm{ref}})A^{-1/2}_{\mathrm{ref}}.$$

We define the square root of a symmetric positive definite matrix $A^{1/2}$ as the unique principal square root, also positive definite. The error indicators are defined with the goal to reduce memory consumption. With the definitions above, all quantities depending on the reference coefficient and right-hand side can be computed in advance. Further implementation details will be discussed in section 5.

The numerical method we propose in the next subsection exploits the possibility to replace, e.g., $\mathcal{R}_{k,T}f$ with the precomputed $\mathcal{R}^{\mathrm{ref}}_{k,T}f_{\mathrm{ref}}$, and to reuse integrals for the stiffness matrix based on A_{ref} instead of using A. The error indicators will be used to identify which local problems need to be recomputed and which local problems can be computed using the reference data.

Remark 3.3 (perturbed boundary data). We do not cover the case when g is perturbed. It can be perturbed explicitly from a reference boundary condition (in which case a reference g similar to f_{ref} needs to be introduced), or it can be perturbed by a domain mapping $g|_\Gamma = g_y \circ \psi$. We remark that if ψ is the identity mapping for all points on the boundary Γ, then g (including its values in the interior of the domain) can be picked independent of ψ.

Remark 3.4 (pure domain mapping). In the domain mapping setting, assuming A_{ref} to be scalar and $D \equiv 0$, we have that

$$\delta = (\det(\mathcal{J})\mathcal{J}^{-1}\mathcal{J}^{-T})^{-1/2}\left(\det(\mathcal{J})\mathcal{J}^{-1}\mathcal{J}^{-T} - \mathrm{Id}\right),$$

i.e., it is independent of A_{ref}. If the Jacobi matrix can be written as a ϵ-perturbation of the identity, the size of δ will be proportional to ϵ.

3.5. Adaptive method. We are now ready to present the full method with adaptively updated correctors. The main idea is to compute the perturbed correctors only for a subset of all elements and reuse the reference correctors for all other elements. This means we effectively solve the problem in a mixed multiscale space using a bilinear form that is defined as a combination of the two coefficients. All elements whose error indicators are smaller than a tolerance TOL will be marked for recomputation. The number of recomputed correctors is thus determined indirectly by this tolerance parameter TOL.

DEFINITION 3.5 (PG-LOD with adaptively updated correctors). *The proposed method follows six steps:*

1. *Pick a tolerance TOL.*
2. *Provided reference data $(A_{\mathrm{ref}}, f_{\mathrm{ref}})$: Compute (for all $T \in \mathcal{T}_H$) reference correctors $\mathcal{Q}^{\mathrm{ref}}_{k,T}\lambda_x$ (for all basis functions λ_x), $\mathcal{R}^{\mathrm{ref}}_{k,T} f_{\mathrm{ref}}$, and $\mathcal{Q}^{\mathrm{ref}}_{k,T} g$, based on the reference coefficient A_{ref} and reference right-hand side f_{ref}.*
3. *Provided perturbed data (A, f): Compute (for all $T \in \mathcal{T}_H$) error indicators $E_{\mathcal{Q}V_H,T}$, $E_{f,T}$, $E_{\mathcal{R}f,T}$, and $E_{\mathcal{Q}g,T}$ and mark the elements T for which all of the following inequalities hold true,*

$$\begin{aligned} E_{\mathcal{Q}V_H,T} &\leq TOL, \\ E_{f,T} + E_{\mathcal{R}f,T} &\leq TOL\left(\|f\|_{L^2(\Omega)} + |||g|||\right), \\ E_{\mathcal{Q}g,T} &\leq TOL\left(\|f\|_{L^2(\Omega)} + |||g|||\right). \end{aligned} \tag{3.10}$$

   Denote the set of marked elements by $\mathcal{T}^{\mathrm{ref}}_H \subset \mathcal{T}_H$.
4. *Compute (for all $T \in \mathcal{T}_H \setminus \mathcal{T}^{\mathrm{ref}}_H$) the mixed correctors $\tilde{\mathcal{Q}}_{k,T}\lambda_x$, $\tilde{\mathcal{Q}}_{k,T} g$, and $\tilde{\mathcal{R}}_{k,T}\tilde{f}$, based on the following definitions of the mixed right-hand side and correctors: $\tilde{f} \in L^2(\Omega)$ and*

$$\tilde{f}|_T = \begin{cases} f_{\mathrm{ref}}|_T, \\ f|_T, \end{cases} \qquad \tilde{\mathcal{Q}}_{k,T} = \begin{cases} \mathcal{Q}^{\mathrm{ref}}_{k,T}, \\ \mathcal{Q}_{k,T}, \end{cases} \qquad \tilde{\mathcal{R}}_{k,T} = \begin{cases} \mathcal{R}^{\mathrm{ref}}_{k,T} & \text{for } T \in \mathcal{T}^{\mathrm{ref}}_H, \\ \mathcal{R}_{k,T} & \text{otherwise.} \end{cases}$$

   Note that only element correctors in $\mathcal{T}_H \setminus \mathcal{T}^{\mathrm{ref}}_H$ need to be recomputed since the reference correctors from item 1 will be used for the elements in $\mathcal{T}^{\mathrm{ref}}_H$. We further let $\tilde{\mathcal{Q}}_k = \sum_{T\in\mathcal{T}_H} \tilde{\mathcal{Q}}_{k,T}$ and $\tilde{\mathcal{R}}_k = \sum_{T\in\mathcal{T}_H} \tilde{\mathcal{R}}_{k,T}$.
5. *Assemble the adaptively updated LOD stiffness matrix*

$$\tilde{K}_{xy} = \tilde{b}(\lambda_y, \lambda_x) \tag{3.11}$$

   using the mixed unsymmetric bilinear form $\tilde{b}$ defined in terms of a element-wise reference b^{ref}_T and a perturbed b_T:

$$\begin{aligned} b^{\mathrm{ref}}_T(v,w) &= (A_{\mathrm{ref}}(\chi_T\nabla - \nabla\mathcal{Q}^{\mathrm{ref}}_{k,T})v\,,\,\nabla w)_{U_k(T)}, \\ b_T(v,w) &= (A(\chi_T\nabla - \nabla\mathcal{Q}_{k,T})v\,,\,\nabla w)_{U_k(T)}, \\ \tilde{b}(v,w) &= \sum_{T\in\mathcal{T}^{\mathrm{ref}}_H} b^{\mathrm{ref}}_T(v,w) + \sum_{T\in\mathcal{T}_H\setminus\mathcal{T}^{\mathrm{ref}}_H} b_T(v,w). \end{aligned}$$

6. *Similarly, define the functional $\tilde{c}$ for the right-hand side correctors by*

$$c_T^{\mathrm{ref}}(v) = (A_{\mathrm{ref}}\nabla\mathcal{R}_{k,T}^{\mathrm{ref}} f_{\mathrm{ref}}\,,\,\nabla v)_{U_k(T)},$$
$$c_T(v) = (A\nabla\mathcal{R}_{k,T} f\,,\,\nabla v)_{U_k(T)},$$
$$\tilde{c}(v) = \sum_{T\in\mathcal{T}_H^{\mathrm{ref}}} c_T^{\mathrm{ref}}(v) + \sum_{T\in\mathcal{T}_H\setminus\mathcal{T}_H^{\mathrm{ref}}} c_T(v)$$

solve for $\tilde{u}_k^H \in V_H$ in

$$\tilde{b}(\tilde{u}_k^H, v) = F(v) - \tilde{c}(v) - \tilde{b}(g, v) \tag{3.12}$$

for all $v \in V_H$, and compute the solution as

$$\tilde{u}_k = \tilde{u}_k^H - \tilde{Q}_k\tilde{u}_k^H + \tilde{\mathcal{R}}_k\tilde{f} - \tilde{Q}_k g. \tag{3.13}$$

Remark 3.6 (individual marking). The described algorithm can be enhanced in terms of efficiency by separating $\mathcal{T}_H^{\mathrm{ref}}$ for each corrector type $\mathcal{Q}_{k,T}\lambda_x$, $\mathcal{R}_{k,T}f$, and $\mathcal{Q}_{k,T}g$, only updating the correctors with respect to their corresponding error indicator. For example, if $A = A_{\mathrm{ref}}$ but $f \neq f_{\mathrm{ref}}$, obviously the f-independent correctors $\mathcal{Q}_{k,T}\lambda_x$ and $\mathcal{Q}_{k,T}g$ need not to be recomputed in item 4, since only $\mathcal{R}_{k,T}f$ can differ from its reference counterpart $\mathcal{R}_{k,T}^{\mathrm{ref}} f_{\mathrm{ref}}$. As stated, however, the algorithm would (unnecessarily) recompute the f-independent correctors as well. For readability of this paper, we decided to omit individual marking.

4. Error analysis. This section is devoted to the theoretical justification of the proposed method. We present the main theorem of this work. The theorem justifies local recomputation of the correctors based on the value of the error indicators.

THEOREM 4.1 (error bound for the PG-LOD with adaptively updated correctors). *There exists $k_0 > 0$ and $\tau_0 > 0$, such that with $TOL = \tau k^{-d/2}$, the error bound*

$$|||u - \tilde{u}_k||| \lesssim k^{d/2}(\theta^k + TOL)(\|f\|_{L^2(\Omega)} + |||g|||) \tag{4.1}$$

is satisfied for all $k > k_0$ and $\tau < \tau_0$ if the error indicators satisfy

$$\max_{T\in\mathcal{T}_H^{\mathrm{ref}}}(E_{\mathcal{Q}V_H,T}\left(\|f\|_{L^2(\Omega)} + |||g|||\right), E_{f,T} + E_{\mathcal{R}f,T}, E_{\mathcal{Q}g,T}) \leq TOL\left(\|f\|_{L^2(\Omega)} + |||g|||\right). \tag{4.2}$$

Here, $0 < \theta < 1$ is independent of H, k, τ, and TOL.

Note that hypothesis (4.2) is directly related to item 3 in Definition 3.5 and is thus automatically satisfied by recomputing correctors that do not fulfill (4.2) as proposed in item 4 of our adaptive method. The factor $k^{-d/2}$ in TOL is necessary to guarantee coercivity of the coarse bilinear form when the size of the patches grow, but this appears not to limit our method in practice.

Before proving the theorem, we require the following lemma.

LEMMA 4.2 (error indicators bound the errors in reference correctors and integrals). *For all $v \in V_H$, the following bounds hold:*

$$|||\mathcal{Q}_{k,T}v - \mathcal{Q}_{k,T}^{\mathrm{ref}}v||| \leq \|A^{-1/2}(A - A_{\mathrm{ref}})(\chi_T\nabla v - \nabla\mathcal{Q}_{k,T}^{\mathrm{ref}}v)\|_{L^2(U_k(T))} \leq E_{\mathcal{Q}V_H,T}|||v|||_T,$$
$$|||\mathcal{R}_{k,T}f - \mathcal{R}_{k,T}^{\mathrm{ref}}f_{\mathrm{ref}}||| \leq E_{f,T} + \|A^{-1/2}(A - A_{\mathrm{ref}})\nabla\mathcal{R}_{k,T}^{\mathrm{ref}}f_{\mathrm{ref}}\|_{L^2(U_k(T))} \leq E_{f,T} + E_{\mathcal{R}f,T},$$
$$|||\mathcal{Q}_{k,T}g - \mathcal{Q}_{k,T}^{\mathrm{ref}}g||| \leq \|A^{-1/2}(A - A_{\mathrm{ref}})(\chi_T\nabla g - \nabla\mathcal{Q}_{k,T}^{\mathrm{ref}}g)\|_{L^2(U_k(T))} \leq E_{\mathcal{Q}g,T}.$$

Proof of Lemma 4.2. For any $v \in V_H$, we define $z := \mathcal{Q}_{k,T} v - \mathcal{Q}^{\mathrm{ref}}_{k,T} v \in V^{\mathrm{f}}(U_k(T))$ and observe

$$\begin{aligned}
\|\!|z|\!\|^2_{U_k(T)} &= (A\nabla v\,,\,\nabla z)_T - (A\nabla \mathcal{Q}^{\mathrm{ref}}_{k,T} v\,,\,\nabla z)_{U_k(T)} \\
&\qquad + (A_{\mathrm{ref}}\nabla \mathcal{Q}^{\mathrm{ref}}_{k,T} v\,,\,\nabla z)_{U_k(T)} - (A_{\mathrm{ref}}\nabla v\,,\,\nabla z)_T \\
&\leq \|A^{-1/2}(A - A_{\mathrm{ref}})(\chi_T \nabla v - \nabla \mathcal{Q}^{\mathrm{ref}}_{k,T} v)\|_{L^2(U_k(T))} \cdot \|\!|z|\!\|_{U_k(T)},
\end{aligned}$$

which yields the first inequality of the first part. We proceed to get the second inequality,

$$\begin{aligned}
\|\!|z|\!\|^2_{U_k(T)} &\leq \|A^{-1/2}(A - A_{\mathrm{ref}})(\chi_T \nabla v - \nabla \mathcal{Q}^{\mathrm{ref}}_{k,T} v)\|^2_{L^2(U_k(T))} \\
&\leq \max_{w|_T,\, w \in V_H} \frac{\|A^{-1/2}(A - A_{\mathrm{ref}})(\chi_T \nabla w - \nabla \mathcal{Q}^{\mathrm{ref}}_{k,T} w)\|^2_{L^2(U_k(T))}}{\|A^{1/2}_{\mathrm{ref}} \nabla w\|^2_{L^2(T)}} \|A^{1/2}_{\mathrm{ref}} \nabla v\|^2_{L^2(T)} \\
&\leq \|A_{\mathrm{ref}} A^{-1}\|_{L^\infty(T)} \\
&\qquad \cdot \sum_{\substack{T' \in \mathcal{T}_H \\ T' \cap U_k(T) \neq 0}} \|\delta\|^2_{L^\infty(T')} \max_{w|_T,\, w \in V_H} \frac{\|A^{1/2}_{\mathrm{ref}}(\chi_T \nabla w - \nabla \mathcal{Q}^{\mathrm{ref}}_{k,T} w)\|^2_{L^2(T')}}{\|A^{1/2}_{\mathrm{ref}} \nabla w\|^2_{L^2(T)}} \|\!|v|\!\|^2_T \\
&= E^2_{\mathcal{Q} V_H, T} \|\!|v|\!\|^2_T
\end{aligned}$$

with $\delta = A^{-1/2}(A - A_{\mathrm{ref}}) A^{-1/2}_{\mathrm{ref}}$.

The second result follows analogously with $z' := \mathcal{R}_{k,T} f - \mathcal{R}^{\mathrm{ref}}_{k,T} f_{\mathrm{ref}} \in V^{\mathrm{f}}(U_k(T))$ and

$$\begin{aligned}
\|\!|z'|\!\|^2_{U_k(T)} &= (f - f_{\mathrm{ref}}\,,\,z')_T + (f_{\mathrm{ref}}\,,\,z')_T - (A\nabla \mathcal{R}^{\mathrm{ref}}_{k,T} f_{\mathrm{ref}}\,,\,\nabla z')_{U_k(T)} \\
&\leq \Big(\|A^{-1}\|^{1/2}_{L^\infty(U(T))} \|f - f_{\mathrm{ref}}\|_{L^2(T)} \sup_{v \in V} \frac{\|(\mathrm{Id} - \mathcal{I}_H) v\|_{L^2(T)}}{\|\nabla v\|_{L^2(U(T))}} \\
&\qquad + \Big(\|A^{-1/2}(A - A_{\mathrm{ref}}) \nabla \mathcal{R}^{\mathrm{ref}}_{k,T} f_{\mathrm{ref}}\|_{L^2(U_k(T))} \Big) \cdot \|\!|z'|\!\|_{U_k(T)}.
\end{aligned}$$

Similar arguments yield the third result of the lemma. ∎

Proof of Theorem 4.1. The full error is $\|\!|u - \tilde{u}_k|\!\| \leq \|\!|u - u_k|\!\| + \|\!|u_k - \tilde{u}_k|\!\|$. The first term stems from the localization and is bounded by $\|\!|u - u_k|\!\| \lesssim k^{d/2}\, \theta^k (\|f\|_{L^2(\Omega)} + \|\!|g|\!\|)$ according to (3.8).

Before proceeding with the second term, we note that we can bound the error in the global correctors $\tilde{\mathcal{Q}}_k$ and $\tilde{\mathcal{R}}_k$ in terms of the patch overlap $k^{d/2}$ and TOL by using Lemma 4.2 and the assumption on TOL stated in this theorem: for all $v \in V_H$,

$$\begin{aligned}
\|\!|(\mathcal{Q}_k - \tilde{\mathcal{Q}}_k) v|\!\|^2 &= \|\!| \textstyle\sum_{T \in \mathcal{T}^{\mathrm{ref}}_H} (\mathcal{Q}_{k,T} - \mathcal{Q}^{\mathrm{ref}}_{k,T}) v |\!\|^2 \\
&\lesssim \textstyle\sum_{T \in \mathcal{T}^{\mathrm{ref}}_H} k^d \|\!|(\mathcal{Q}_{k,T} - \mathcal{Q}^{\mathrm{ref}}_{k,T}) v|\!\|^2 \\
&\lesssim k^d \mathrm{TOL}^2 \|\!|v|\!\|^2.
\end{aligned} \tag{4.3}$$

Analogously, we get $\|\!|(\mathcal{R}_k - \tilde{\mathcal{R}}_k) f|\!\| + \|\!|(\mathcal{Q}_k - \tilde{\mathcal{Q}}_k) g|\!\| \lesssim k^{d/2} \mathrm{TOL}(\|f\|_{L^2(\Omega)} + \|\!|g|\!\|)$. Using (3.7) and (4.3), we additionally bound

$$\|\!|\tilde{\mathcal{Q}}_k v|\!\| = \|\!|\mathcal{Q} v|\!\| + \|\!|(\mathcal{Q} - \mathcal{Q}_k) v|\!\| + \|\!|(\mathcal{Q}_k - \tilde{\mathcal{Q}}_k) v|\!\| \lesssim (1 + k^{d/2}\theta^k + k^{d/2}\mathrm{TOL}) \|\!|v|\!\| \lesssim \|\!|v|\!\|.$$

Next, we proceed with the second term, using (3.6) and (3.13) and the bounds above,

(4.4)
$$\begin{aligned}|||u_k - \tilde{u}_k||| &\le |||u_k^H - \tilde{u}_k^H||| + |||\mathcal{Q}_k u_k^H - \tilde{\mathcal{Q}}_k \tilde{u}_k^H||| + |||\mathcal{R}_k f - \tilde{\mathcal{R}}_k \tilde{f}||| - |||\mathcal{Q}_k g - \tilde{\mathcal{Q}}_k g||| \\ &\lesssim |||u_k^H - \tilde{u}_k^H||| + |||\mathcal{Q}_k u_k^H - \tilde{\mathcal{Q}}_k u_k^H||| + |||\mathcal{R}_k f - \tilde{\mathcal{R}}_k \tilde{f}||| - |||\mathcal{Q}_k g - \tilde{\mathcal{Q}}_k g||| \\ &\lesssim |||u_k^H - \tilde{u}_k^H||| + k^{d/2}\mathrm{TOL}(\|f\|_{L^2(\Omega)} + |||g|||),\end{aligned}$$

where we added $\pm\tilde{\mathcal{Q}}_k u_k^H$ in the second estimate and use $|||u_k^H||| \lesssim \|f\|_{L^2(\Omega)} + |||g|||$ for the last step.

It remains to bound the energy norm of $u_k^H - \tilde{u}_k^H \in V_H$. The first step is to establish a coercivity inequality for $\tilde{b}$ on V_H. To do this, we define the auxiliary bilinear form $b = \sum_{T\in\mathcal{T}_H} b_T$ (with b_T defined in Definition 3.5) and bound the consistency error $[b - \tilde{b}](v, w)$ for $v, w \in V_H$,

$$[b - \tilde{b}](v, w) = \sum_{T\in\mathcal{T}_H^{\mathrm{ref}}} [b_T^{\mathrm{ref}} - b_T](v, w) \lesssim k^{d/2}\mathrm{TOL}|||v|||\,|||w|||, \tag{4.5}$$

since

$$\begin{aligned}[b_T^{\mathrm{ref}} - b_T](v, w) &= (A_{\mathrm{ref}}(\chi_T\nabla - \nabla\mathcal{Q}_{k,T}^{\mathrm{ref}})v - A(\chi_T\nabla - \nabla\mathcal{Q}_{k,T})v\,,\,\nabla w)_{U_k(T)} \\ &= ((A_{\mathrm{ref}} - A)(\chi_T\nabla - \nabla\mathcal{Q}_{k,T}^{\mathrm{ref}})v - A\nabla(\mathcal{Q}_{k,T} - \mathcal{Q}_{k,T}^{\mathrm{ref}})v\,,\,\nabla w)_{U_k(T)} \\ &\le \|A^{-1/2}(A_{\mathrm{ref}} - A)(\chi_T\nabla - \nabla\mathcal{Q}_{k,T}^{\mathrm{ref}})v\|_{L^2(U_k(T))}|||w|||_{U_k(T)} \\ &\quad + |||(\mathcal{Q}_{k,T} - \mathcal{Q}_{k,T}^{\mathrm{ref}})v|||\,|||w|||_{U_k(T)} \\ &\lesssim \mathrm{TOL}|||v|||_T|||w|||_{U_k(T)},\end{aligned}$$

where we again use Lemma 4.2. Additionally, for $v \in V_H$, we note that

(4.6)
$$a(v - \mathcal{Q}v, v) = a(v - \mathcal{Q}v, v - \mathcal{Q}v) = |||v - \mathcal{Q}v|||^2 \ge \alpha\beta^{-1}C_{\mathcal{I}_H}^{-2}|||\mathcal{I}_H(v - \mathcal{Q}v)|||^2 \gtrsim |||v|||^2,$$

and further that $a(v - \mathcal{Q}_k v, v) = b(v, v)$. Using (4.6), (3.7), (4.5), and the triangle inequality, we get for $v \in V_H$,

$$\begin{aligned}|\tilde{b}(v, v)| &\ge a(v - \mathcal{Q}v, v) - |a((\mathcal{Q} - \mathcal{Q}_k)v, v)| - |[b - \tilde{b}](v, v)| \\ &\ge (C_1 - C_2k^{d/2}\theta^k - C_3k^{d/2}\mathrm{TOL})|||v|||^2,\end{aligned}$$

where C_1, C_2, and C_3 are independent of H, k, and TOL. From this inequality, we note that there exist k_0 and τ_0 such that, for all $k > k_0$ and $\tau < \tau_0$ (with $\mathrm{TOL} = \tau k^{-d/2}$), we have the coercivity inequality

$$\tilde{b}(v, v) \ge \tilde{\gamma}|||v|||^2 \gtrsim |||v|||^2$$

for all $v \in V_H$, where $\tilde{\gamma}$ depends on k_0 and τ_0 but not on H, k, τ or TOL.

We define $c = \sum_{T\in\mathcal{T}_H} c_T$ and observe that the localized problem (3.5) can be expressed in the same manner as the proposed approximation in (3.12) as

$$b(u_k^H, v) = F(v) - c(v) - b(g, v)$$

for all $v \in V_H$. Next, we use the coercivity inequality with $v = u_k^H - \tilde{u}_k^H =: e \in V_H$

and the reformulation of (3.5) together with (3.12) to obtain

$$
\begin{aligned}
\|\!|u_k^H - \tilde{u}_k^H|\!\|^2 &\lesssim \tilde{b}(u_k^H - \tilde{u}_k^H, e) = \tilde{b}(u_k^H, e) - F(e) + \tilde{c}(e) + \tilde{b}(g, e) \\
&= [\tilde{b} - b](u_k^H, e) + [\tilde{c} - c](e) + [\tilde{b} - b](g, e) \\
&\lesssim k^{d/2}\mathrm{TOL}(\|\!|u_k^H|\!\| + \|f\|_{L^2(\Omega)} + \|\!|g|\!\|)\|\!|e|\!\| \\
&\lesssim k^{d/2}\mathrm{TOL}(\|f\|_{L^2(\Omega)} + \|\!|g|\!\|)\|\!|u_k^H - \tilde{u}_k^H|\!\|,
\end{aligned} \tag{4.7}
$$

where we used (4.5) for $[\tilde{b} - b](u_k^H, e)$ (and analogously derived results for $[\tilde{c} - c](e)$ and $[\tilde{b} - b](g, e)$). Combining the last bound with (3.8) and (4.4) yields the asserted bound. ∎

Remark 4.3 ($V = H_0^1(\Omega)$). The assumption that $V = V_h$ (a finite element space) means that the error will be with respect to the finite element approximation $u \in V_h$. The same analysis goes through if we instead let $V = H_0^1(\Omega)$ but the corresponding continuous solution is not computable. It is assumed that there is a fine mesh with mesh size h for which the error in the fine scale finite element solution is small enough. An additional a priori error bound then gives the full error with respect to the continuous solution using the triangle inequality.

5. Implementation. This section discusses implementation details specific to the presented method, with emphasis on the computation of the error indicators, parallel computations, and memory consumption for large-scale problems. For implementation details on the LOD corrector problems we refer to [9]. However, we would like to emphasize that the localized computations of correctors on patches makes it possible to avoid any global computations in the (typically very large) space V_h.

5.1. Computing the error indicators. It is important for the method that the local error indicators $E_{\mathcal{Q}V_H,T}$, $E_{f,T}$, $E_{\mathcal{R}f,T}$, and $E_{\mathcal{Q}g,T}$ can be computed efficiently. Consider the definition of $E_{\mathcal{Q}V_H,T}$ from (3.9):

$$
\begin{aligned}
E_{\mathcal{Q}V_H,T}^2 &:= \|A_{\mathrm{ref}}A^{-1}\|_{L^\infty(T)} \\
&\quad \cdot \sum_{\substack{T' \in \mathcal{T}_H \\ T' \cap U_k(T) \neq 0}} \|\delta\|_{L^\infty(T')}^2 \underbrace{\max_{w|_T,\, w \in V_H} \frac{\|A_{\mathrm{ref}}^{1/2}(\chi_T \nabla w - \nabla \mathcal{Q}_{k,T}^{\mathrm{ref}} w)\|_{L^2(T')}^2}{\|A_{\mathrm{ref}}^{1/2}\nabla w\|_{L^2(T)}^2}}_{=:\tilde{\mu}_{T,T'}}.
\end{aligned}
$$

We denote the maximum factor by $\tilde{\mu}_{T,T'}$ and note that computing the error corrector for an element T amounts to computing $\|A_{\mathrm{ref}}A^{-1}\|_{L^\infty(T)}$, and additionally $\|\delta\|_{L^\infty(T')}^2 = \|A^{-1/2}(A_{\mathrm{ref}} - A)A_{\mathrm{ref}}^{-1/2}\|_{L^\infty(T')}^2$ and $\tilde{\mu}_{T,T'}$ for the coarse elements T' in the patch $U_k(T)$. The values $\tilde{\mu}_{T,T'}$ can be precomputed as $\tilde{\mu}_{T,T'} = \max_l \mu_l$, where μ_l is the solution of the eigenvalue problem

$$
\mathcal{B}x_l = \mu_l \mathcal{C}x_l \tag{5.1}
$$

with

$$
\begin{aligned}
\mathcal{B}_{ij} &= \left((A_{\mathrm{ref}}(\chi_T \nabla\lambda_j - \nabla\mathcal{Q}_{k,T}^{\mathrm{ref}}\lambda_j)\,,\, \chi_T\nabla\lambda_i - \nabla\mathcal{Q}_{k,T}^{\mathrm{ref}}\lambda_i\right)_{T'}, \\
\mathcal{C}_{ij} &= \left(A_{\mathrm{ref}}\nabla\lambda_j\,,\, \nabla\lambda_i\right)_T
\end{aligned} \tag{5.2}
$$

for $i, j = 1, \ldots, m-1$ and where m denotes the number of basis functions with support in element T. For two dimensional (2D) quadrilateral mesh elements this results in

a 3×3 system. Given a perturbed coefficient A, we then have to compute only the $\|\delta\|^2_{L^\infty(T')}$ terms and multiply them with the precomputed $\tilde{\mu}_{T,T'}$ before summing, and also computing the $\|A_{\text{ref}}A^{-1}\|_{L^\infty(T)}$ factor. An important consequence of this procedure is that the fine scale reference correctors $\mathcal{Q}^{\text{ref}}_{k,T}\lambda_j$ can be discarded and only the coarse scale quantity $\tilde{\mu}_{T,T'}$ needs to be stored.

The error indicator $E_{\mathcal{Q}g,T}$ for $\mathcal{Q}^{\text{ref}}_{k,T}g$ can be computed in a similar way as $E_{\mathcal{Q}V_H,T}$, the difference being that no eigenvalue problem over functions in V_H restricted to T needs to be solved since g is known a priori.

The right-hand side error indicator $E_{f,T} + E_{\mathcal{R}f,T}$ is slightly different, since perturbations of both f and A affect the accuracy of $\mathcal{R}^{\text{ref}}_{k,T}f_{\text{ref}}$. The second term $E_{\mathcal{R}f,T}$ can be computed similarly to $E_{\mathcal{Q}V_H,T}$ and $E_{\mathcal{Q}g,T}$. The first term $E_{f,T}$ contains an element local Poincaré-type inequality for functions in the fine space (i.e., the null space of $\mathcal{I}_H$),

$$\nu_T := \sup_{v \in V} \frac{\|(\text{Id} - \mathcal{I}_H)v\|_{L^2(T)}}{\|\nabla v\|_{L^2(U(T))}}. \tag{5.3}$$

We have from the a priori approximability bound of $\mathcal{I}_H$ in (3.1) that this quantity scales with H. If the constant $C_{\mathcal{I}_H}$ is known, it can be used here. In many practical situations it is possible to get a sharp estimate by computational means since V is the finite element space V_h and the bound we seek is the maximum eigenvalue to a problem posed on a 1-layer element patch $U(T)$ on the fine scale. For all the experiments in section 6 we discretize the 2D unit square with a uniform grid and get three possible cases: $U(T)$ consists of 4, 6, or 9 elements (depending on whether it is in the corner, on the edge, or in the interior of the domain). By computing (5.3) with $V = V_h$ for a decreasing range of small h, it was possible to obtain the estimate $\nu_T \leq 0.25H$ for all T. This value was used in the experiments in section 6.

5.2. Algorithm, parallelization, and memory consumption. Algorithm 5.1 shows an example of how the computational steps can be carried out. It is based on the assumption that we have to solve for multiple perturbations of a certain reference coefficient and therefore consists of an initial stage when reference quantities are computed. We make the following observations:

- The amount of data stored from the initial stage scales like $k^d H^{-d}$ since it consists only of overlapping quantities on the coarse mesh.
- The initial stage can be computed in parallel over T thanks to the PG-LOD formulation since $b^{\text{ref}}_T(\lambda_j, \lambda_i)$, $c^{\text{ref}}_T(\lambda_i)$, and $b^{\text{ref}}_T(g, \lambda_i)$ depend only on the correctors for T.

Following the initial stage, a loop over the perturbed coefficients follows. For each perturbed coefficient, there is another loop over the elements T. It computes updated correctors for the elements for which the error indicators say it is needed. Finally, the coarse scale linear system is assembled and solved and the full solution can be computed. We note the following:

- The iterations in the loop over the perturbed coefficients can be executed in parallel.
- The iterations in the loop over the elements T can be executed in parallel.
- In order to compute the error indicators, the reference coefficient A_{ref} needs to either be stored explicitly (amount h^{-d}), be transmitted patchwise (amount $k^d(h/H)^{-d}$) between computers, or be generated from a low-dimensional representation on demand.

Algorithm 5.1 Procedure of the proposed method.

Input: Reference data $(A_{\text{ref}}, f_{\text{ref}})$
Pick k and TOL
for all T **do**
  Precompute $\mathcal{Q}^{\text{ref}}_{k,T}\lambda_j$, $\mathcal{R}^{\text{ref}}_{k,T}f_{\text{ref}}$, and $\mathcal{Q}^{\text{ref}}_{k,T}g$ for all j (discard at end of iteration)
  Precompute and save ν_T and $\tilde{\mu}_{T,T'}$ for all $T' \subset U_k(T)$
  Precompute and save $b^{\text{ref}}_T(\lambda_j, \lambda_i)$, $c^{\text{ref}}_T(\lambda_i)$, and $b^{\text{ref}}_T(g, \lambda_i)$ for all i and j
end for
for perturbed data (A, f) **do**
  $\mathcal{T}^{\text{ref}}_H \leftarrow \emptyset$
  for all T **do**
    Compute $E_{\mathcal{Q}V_H,T}$, $E_{f,T}$, $E_{\mathcal{R}f,T}$, and $E_{\mathcal{Q}g,T}$ using $\tilde{\mu}_{T,T'}$, and ν_T
    if $\max(E_{\mathcal{Q}V_H,T}(\|f\|_{L^2(T)} + \|\!|g|\!\|), E_{f,T}, E_{\mathcal{R}f,T}, E_{\mathcal{Q}g,T}) \leq \text{TOL}$ **then**
      $\mathcal{T}^{\text{ref}}_H \leftarrow \{T\} \cup \mathcal{T}^{\text{ref}}_H$
      Compute $\mathcal{Q}_{k,T}\lambda_j$ for all j, $\mathcal{R}_{k,T}f$, and $\mathcal{Q}_{k,T}g$ (discard at end of iteration)
      Compute and save $b_T(\lambda_j, \lambda_i)$, $c_T(\lambda_i)$, and $b_T(g, \lambda_i)$ for all i and j
    end if
  end for
  Assemble stiffness matrix $\tilde{K}_{i,j} = \sum_{T\in\mathcal{T}^{\text{ref}}_H} b^{\text{ref}}_T(\lambda_j, \lambda_i) + \sum_{T\notin\mathcal{T}^{\text{ref}}_H} b_T(\lambda_j, \lambda_i)$ and load vector similarly
  Solve for $\tilde{u}^H_k$ using (3.12)
  Possibly compute full solution by $\tilde{u}_k = (\text{Id} - \tilde{\mathcal{Q}}_k)\tilde{u}^H_k - \tilde{\mathcal{Q}}_k g + \tilde{\mathcal{R}}_k \tilde{f}$
end for

- There is a reduction over T to assemble the stiffness matrix and the load vector, but only coarse scale data of amount $k^d H^{-d}$ is needed for this reduction. This means that fine scale information does not need to be transmitted between computers during reduction.
- The coarse scale solution $\tilde{u}^H_k$ is readily available after solving the coarse scale linear system. If the full solution $\tilde{u}_k$ is requested in some area of the domain, the correctors in that area have to be recomputed or stored from a previous corrector computation.

Remark 5.1 (periodicity). Applications such as composite materials often lead to a periodic structure of the underlying reference coefficient. In this case, correctors can be reused. In the full periodic case this leads to only one corrector problem for full patches and comparably few for the boundary patches. This means that memory consumption as well as complexity decreases significantly.

6. Numerical experiments. We present three experiments where the diffusion coefficient is perturbed by defects with either no domain mapping, local domain mapping, or global domain mapping. We performed this experiments with `gridlod` in Python (see [13]). The entire code for this section is available on GitHub in [14]. Our experiments are performed on a 2D quadrilateral mesh on $\Omega = [0, 1]^2$. For the fine and the coarse scale discretization V_h and V_H, we use standard $\mathcal{P}_1$ finite element spaces on a fine mesh $\mathcal{T}_h$ with 256×256 fine elements and a coarse mesh $\mathcal{T}_H$ with 32×32 coarse elements. We use V_h for the fine reference solution and for the fine scale discretization of each corrector problem. For the mesh size $H = 1/32$ we conclude from the error estimate (3.8) that the localization parameter $k = 4 \geq |\log(H)|$ suffices.

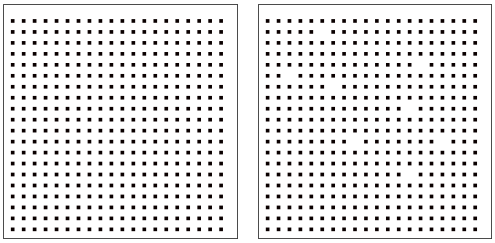

(a) (b)

FIG. 5. *Reference coefficient A_{ref} (left) and defect perturbation A (right). Black is* 1*; white is* 0.1.

In all experiments we use a reference coefficient that is piecewise constant on every fine mesh element. In the first experiment, A_{ref} can be expressed as stated in (2.7), i.e., it takes two values 1 and α. This condition will be relaxed in the second and third experiment as it does not restrict our method to be applicable. The domain Ω_1 represents small changes in the reference coefficient as it is a nonconnected subdomain of Ω which is conforming with respect to $\mathcal{T}_h$. For the sake of convenience we neglect an explicit definition of A_{ref} and A as we visualize them in the figures. We call a perturbation a (local) defect when a (fully connected) subdomain of Ω_1 becomes a subdomain of Ω_α. In all our experiments Ω_1 is represented by squares and a defect means that a square gets equalized to the respective background (compare Figure 5). For all experiments, these defects occur with a probability of 2% and the right-hand side f_y is defined by $f_y(y) = \chi_{[1/8,7/8]^2}(y)$. For the sake of simplicity we use zero Dirichlet boundary conditions $g \equiv 0$.

In the experiments we consider the relative error

$$\mathcal{E}_{\text{rel}}(\tilde{u}_k, u_k) = \frac{|||\tilde{u}_k - u_k|||}{|||\tilde{u}_k|||},$$

where u_k is the best PG-LOD solution of (3.6) and $\tilde{u}_k$ is the solution of (3.13) for a specific tolerance TOL in the algorithm of Definition 3.5. With respect to item 3 in Definition 3.5, we clearly have 0% updates of the correctors for TOL $= \infty$, whereas TOL $= 0$ corresponds to 100% updates. For 100% updates we then end up with the standard Petrov–Galerkin LOD error that is dependent on our data and discretizations. In order to observe the complete behavior of $\mathcal{E}_{\text{rel}}(u_k, \tilde{u}_k)$, we compute it for every possible choice of TOL (and thus for every percentage of updates). The relative best PG-LOD error $\mathcal{E}_{\text{rel}}(u, u_k)$ is always around 10^{-3}, which means that we are comparing to a sufficiently accurate solution.

6.1. Defects. In the first experiment we let $\psi = \text{Id}$, which means we only consider defects and for the background Ω_α we choose $\alpha = 0.1$. Figure 5 displays the coefficient and its perturbation whereas the error indicators $E_{\mathcal{Q}V_H,T}$ and $E_{\mathcal{R}f,T}$ are plotted for each T in Figure 6. Note that $E_{f,T}$ and $E_{\mathcal{Q}g,T}$ are zero for this example. The coarse mesh is visible in the background. We can clearly see that the error indicator $E_{\mathcal{Q}V_H,T}$ detects the defects in the coefficient correctly. Furthermore $E_{\mathcal{Q}V_H,T}$ is exponentially decaying away from each defect. In view of $E_{\mathcal{R}f,T}$, we see that its support coincides with the support of f_{ref} since for $\psi = \text{Id}$ we have $f = f_{\text{ref}}$, which means that whenever f is zero on T, both $\mathcal{R}_{k,T}$ and $\mathcal{R}^{\text{ref}}_{k,T}$ are zero and thus $E_{\mathcal{R}f,T} = 0$. We

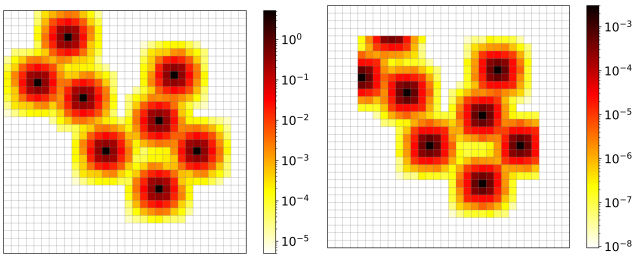

FIG. 6. *Error indicators* $E_{\mathcal{Q}V_H,T} \cdot \|f\|_{L^2(\Omega)}$ *(left) and* $E_{\mathcal{R}f,T}$ *(right).*

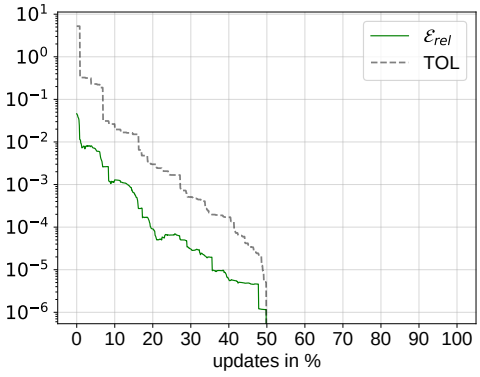

FIG. 7. *Relative error improvement for defects.*

also observe that $E_{\mathcal{Q}V_H,T}$ is significantly greater than $E_{\mathcal{R}f,T}$. In Figure 7 we see a fast convergence of $\mathcal{E}_{\text{rel}}(u_k, \tilde{u}_k)$ for a few updates of the correctors.

6.2. Local domain mappings. In the second experiment, we add domain mappings and neglect the assumption in (2.7) on A_{ref} to demonstrate the widened applicability of our adaptive method. We choose A_{ref} to consist of differently sized and valued particles with values in $[10^0, 5 \cdot 10^0]$ (to replace Ω_1) and a noisy background with values in $[10^{-2}, 5 \cdot 10^{-1}]$ (instead of one value α). See Figure 8 (left) for a visualization of A_{ref}. For the physical perturbed coefficient (Figure 8, middle), we choose ψ to be a local distortion in the middle of the domain and we apply random defects to the particles. With the help of domain mappings the reference coefficient A_{ref} can be mapped to a simple change in value, which means that Ω_1 does not change its position (see Figure 8, right). In the middle of the mapped coefficient A, the circle of the domain mapping is recognizable. Again, Figure 9 visualizes the corresponding error indicators. The domain mapping as well as the defects are clearly notable in $E_{\mathcal{Q}V_H,T}$, whereas the defects stick out compared to the domain mapping. Importantly, f is a distortion of $f_{\text{ref}} = f_y$, which means that the support of the two is not equal (see $E_{f,T}$ in Figure 9). Furthermore f is not affected by the defects in A, and thus $E_{f,T}$ only detects the domain mapping. From Figure 10, we observe a good behavior of the relative error. However, due to the domain mapping and the increased contrast in this experiment, the method takes comparatively longer to converge to the optimal PG-LOD solution. Since A_{ref} does not fulfill the assumption in (2.7), we conclude

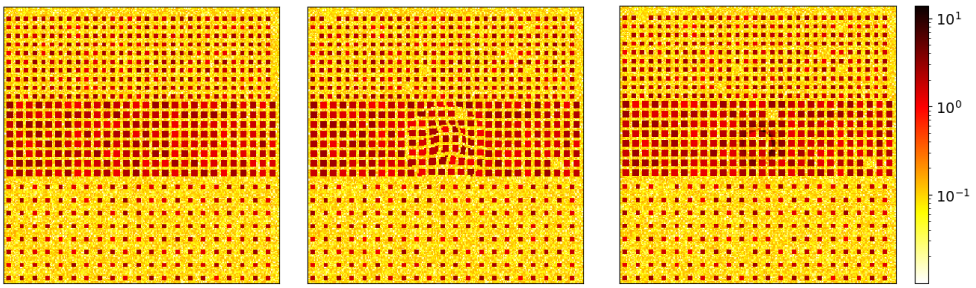

FIG. 8. *Reference coefficient A_{ref} (left), perturbation in the physical domain A_y (center), and corresponding change in value perturbation A (right).*

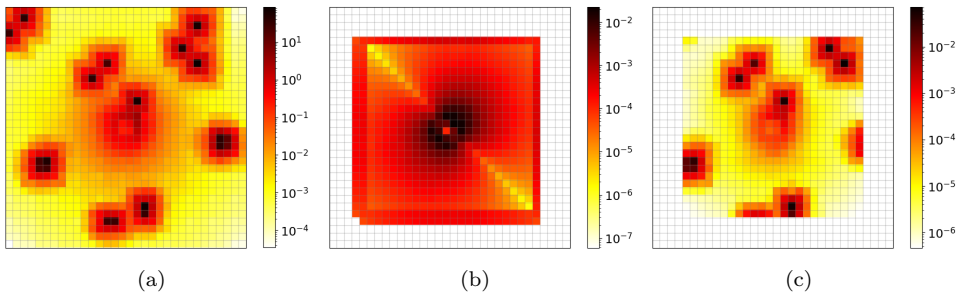

FIG. 9. *Error indicators $E_{\mathcal{Q}V_H,T} \cdot \|f\|_{L^2(\Omega)}$ (left), $E_{f,T}$ (center), and $E_{\mathcal{R}f,T}$ (right).*

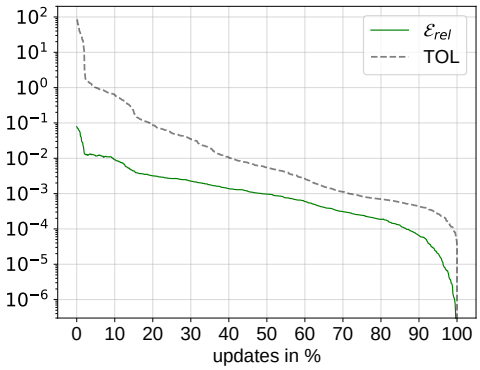

FIG. 10. *Relative error improvement for local domain mapping.*

that the adaptive method is also valid for a big variety of problems, governed by noise or with more complex and less periodic reference structure.

6.3. Global domain mapping. In our third experiment we address the situation that ψ has support on the whole domain Ω. We again consider the same reference coefficient A_{ref} as in section 6.2. Inspired by the domain mapping example in Figure 1 (right) we slightly deform A_{ref} to the right-hand side of the domain. The perturbation

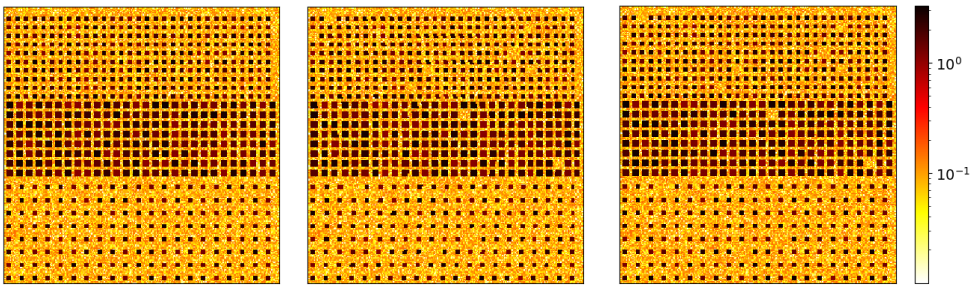

(a) (b) (c)

FIG. 11. *Reference coefficient A_{ref} (left), perturbation in the physical domain A_y (center), and corresponding change in value perturbation A (right).*

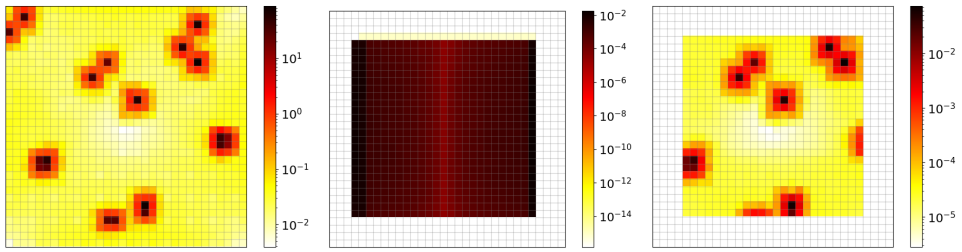

(a) (b) (c)

FIG. 12. *Error indicators $E_{\mathcal{Q}V_H,T} \cdot \|f\|_{L^2(\Omega)}$ (left), $E_{f,T}$ (center), and $E_{\mathcal{R}f,T}$ (right).*

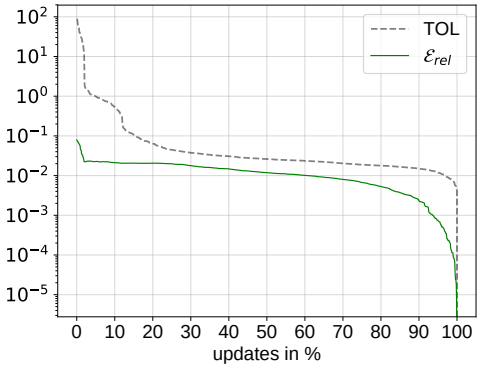

FIG. 13. *Relative error improvement for global domain mapping.*

in the physical domain as well as the change in value of the reference coefficient can be seen in Figure 11. The yellow background in $E_{\mathcal{Q}V_H,T}$ in Figure 12 visualizes the effect of the domain mapping and the defects are clearly notable. In $E_{f,T}$ we once again see the change of support in f (left and right black channel) and the defects are visible in $E_{\mathcal{R}f,T}$.

In Figure 13, we observe that local defects are still resolved efficiently whereas the global map causes a relatively low convergence to the optimal PG-LOD solution.

Thus, this example shows that global domain mappings are difficult to handle. However, for instance, for the case that an accuracy of 10^{-2} is accurate enough, we still get a reasonable result. Note that in this particular example no use of domain mappings would surely result in 100% recomputation as the complete coefficient changes.

Remark 6.1 (choosing TOL). In all our experiments, $\mathcal{E}_{\mathrm{rel}}(u_k, \tilde{u}_k)$ shows a promising behavior. However, we point out that in practice, we clearly do not know $\mathcal{E}_{\mathrm{rel}}(u_k, \tilde{u}_k)$ a priori. Thus, we start with a rather high tolerance TOL and consider an update error $\mathcal{E}_{\mathrm{rel}}(\tilde{u}_{k,\mathrm{old}}, \tilde{u}_k)$, where $\tilde{u}_{k,\mathrm{old}}$ denotes on old approximation with respect to the former tolerance. Whenever the number of updates from one tolerance to another is strictly positive and $\mathcal{E}_{\mathrm{rel}}(\tilde{u}_{k,\mathrm{old}}, \tilde{u}_k)$ does still exhibit a significant gain, we should proceed with a smaller TOL and continue this algorithm until $\mathcal{E}_{\mathrm{rel}}(\tilde{u}_{k,\mathrm{old}}, \tilde{u}_k)$ is small enough.

REFERENCES

[1] I. Babuska and R. Lipton, *Optimal local approximation spaces for generalized finite element methods with application to multiscale problems*, Multiscale Model. Simul., 9 (2011), pp. 373–406, https://doi.org/10.1137/100791051.

[2] X. Blanc, C. Le Bris, and P.-L. Lions, *Une variante de la théorie de l'homogénéisation stochastique des opérateurs elliptiques (a variant of stochastic homogenization theory for elliptic operators)*, C. R. Acad. Sci. Sér. I, 343 (2006), pp. 717–727.

[3] X. Blanc, C. Le Bris, and P.-L. Lions, *Stochastic homogenization and random lattices*, J. Math. Pures Appl., 88 (2007), pp. 34–63.

[4] S. Brenner and R. Scott, *The Mathematical Theory of Finite Element Methods*, Texts Appl. Math. 15, Springer, New York, 2007, https://doi.org/10.1007/978-0-387-75934-0.

[5] J. E. Castrillon-Candas, F. Nobile, and R. F. Tempone, *Analytic regularity and collocation approximation for elliptic pdes with random domain deformations*, Comput. Math. Appl., 71 (2016), pp. 1173–1197, https://doi.org/10.1016/j.camwa.2016.01.005.

[6] P. G. Ciarlet and P.-A. Raviart, *The combined effect of curved boundaries and numerical integration in isoparametric finite element methods*, in The Mathematical Foundations of the Finite Element Method with Applications to Partial Differential Equations, Elsevier, New York, 1972, pp. 409–474.

[7] W. E, B. Engquist, and Z. Huang, *Heterogeneous multiscale method: A general methodology for multiscale modeling*, Phys. Rev. B, 67 (2003), 092101.

[8] D. Elfverson, V. Ginting, and P. Henning, *On multiscale methods in Petrov–Galerkin formulation*, Numer. Math., 131 (2015), pp. 643–682, https://doi.org/10.1007/s00211-015-0703-z.

[9] C. Engwer, P. Henning, A. Målqvist, and D. Peterseim, *Efficient implementation of the localized orthogonal decomposition method*, Comput. Methods Appl. Mechanics Engrg., (2019), https://doi.org/10.1016/j.cma.2019.02.040.

[10] B. Florijn, C. Coulais, and M. van Hecke, *Programmable mechanical metamaterials*, Phys. Rev. Lett., 113 (2014), 175503.

[11] D. Gallistl and D. Peterseim, *Stable multiscale Petrov–Galerkin finite element method for high frequency acoustic scattering*, Comput. Methods Appl. Mech. Engrg., 295 (2015), pp. 1–17, https://doi.org/10.1016/j.cma.2015.06.017.

[12] H. Harbrecht, M. Peters, and M. Siebenmorgen, *Analysis of the domain mapping method for elliptic diffusion problems on random domains*, Numer. Math., 134 (2016), pp. 823–856, https://doi.org/10.1007/s00211-016-0791-4.

[13] F. Hellman and T. Keil, *Gridlod*, https://github.com/fredrikhellman/gridlod.

[14] F. Hellman and T. Keil, *Gridlod-on-perturbations-super*, https://github.com/gridlod-community/gridlod-on-perturbations-super.

[15] F. Hellman and A. Målqvist, *Contrast independent localization of multiscale problems*, Multiscale Model. Simul., 15 (2017), pp. 1325–1355, https://doi.org/10.1137/16M1100460.

[16] F. Hellman and A. Målqvist, *Numerical homogenization of elliptic PDEs with similar coefficients*, Multiscale Model. Simul., 17 (2019), pp. 650–674, https://doi.org/10.1137/18M1189701.

[17] P. Henning and A. Målqvist, *Localized orthogonal decomposition techniques for boundary value problems*, SIAM J. Sci. Comput., 36 (2014), pp. A1609–A1634, https://doi.org/10.1137/130933198.

[18] T. Y. Hou and X.-H. Wu, *A multiscale finite element method for elliptic problems in composite materials and porous media*, J. Comput. Phys., 134 (1997), pp. 169–189, https://doi.org/10.1006/jcph.1997.5682.
[19] T. J. Hughes, G. R. Feijóo, L. Mazzei, and J.-B. Quincy, *The variational multiscale method—A paradigm for computational mechanics*, Comput. Methods Appl. Mech. Engrg., 166 (1998), pp. 3–24, https://doi.org/10.1016/S0045-7825(98)00079-6.
[20] T. Keil, *Variational Crimes in the Localized Orthogonal Decomposition Method*, Master's Thesis, Chalmers University of Technology, Gothenburg, Sweden, 2018.
[21] C. Le Bris, *Some numerical approaches for weakly random homogenization*, in Numerical Mathematics and Advanced Applications 2009, Springer, New York, 2010, pp. 29–45.
[22] C. Le Bris, F. Legoll, and F. Thomines, *Multiscale finite element approach for "weakly" random problems and related issues*, ESAIM Math. Model. Numer. Anal., 48 (2014), pp. 815–858, https://doi.org/10.1051/m2an/2013122.
[23] A. Målqvist and D. Peterseim, *Localization of elliptic multiscale problems*, Math. Comp., 83 (2014), pp. 2583–2603, https://doi.org/10.1090/S0025-5718-2014-02868-8.
[24] A. Målqvist and D. Peterseim, *Computation of eigenvalues by numerical upscaling*, Numer. Math., 130 (2015), pp. 337–361, https://doi.org/10.1007/s00211-014-0665-6.
[25] H. Owhadi and L. Zhang, *Gamblets for opening the complexity-bottleneck of implicit schemes for hyperbolic and parabolic ODEs/PDEs with rough coefficients*, J. Comput. Phys., 347 (2017), pp. 99–128, https://doi.org/10.1016/j.jcp.2017.06.037.
[26] D. Peterseim, *Variational multiscale stabilization and the exponential decay of fine-scale correctors*, in Building Bridges: Connections and Challenges in Modern Approaches to Numerical Partial Differential Equations, Springer, New York, 2016, pp. 343–369.
[27] D. Peterseim and R. Scheichl, *Robust numerical upscaling of elliptic multiscale problems at high contrast*, Comput. Methods Appl. Math., 16 (2016), pp. 579–603, https://doi.org/10.1515/cmam-2016-0022.
[28] L. Wang and K. Bertoldi, *Mechanically tunable phononic band gaps in three-dimensional periodic elastomeric structures*, Internat. J. Solids Structures, 49 (2012), pp. 2881–2885.
[29] D. Xiu and D. Tartakovsky, *Numerical methods for differential equations in random domains*, SIAM J. Sci. Comput., 28 (2006), pp. 1167–1185.
[30] X. Yu, J. Zhou, H. Liang, Z. Jiang, and L. Wu, *Mechanical metamaterials associated with stiffness, rigidity and compressibility: A brief review*, Multiscale Model. Simul., 94 (2018), pp. 114–173.